Journal of Information Systems Engineering and Management
2025, 10(37s)
e-ISSN: 2468-4376
https://www.jisem-journal.com/

Research Article

Modern Control Techniques for Enhancement of Voltage Sag in a MMC Coupled DFIG Based Wind Systems

Sarahath Saleem[1], T. Anil Kumar[2]
[1] Research Scholar, Anurag University, Hyderabad.
[2]School of Engineering, Anurag University, Hyderabad.

ARTICLE INFO

Received: 18 Dec 2024
Revised: 10 Feb 2025
Accepted: 28 Feb 2025

ABSTRACT

Fractional Order Sliding Mode Controller (FOSMC) is a hybrid one and has been integrated to escalate low voltage ride through (LVRT) during faults in a modular multilevel converter (MMC) based doubly fed induction generator (DFIG) connected wind energy conversion system (WECS). Voltage sag at grid directly affects stator of DFIG, due to its immediate connection. The machine's rotor is joined to power electronic converters i.e. a rectifier (MSC) and an inverter (GSC) via a DC link. A Fractional Order Sliding Mode controller is used at Grid Side Converter to mitigate fault current and ameliorate parameters at stator, rotor terminals. This paper infers that proposed Fractional Order Super Twisting Algorithm (FOSTA) deployed Sliding Mode Controller (FOSMC) is the exceptional in dealing with symmetrical and asymmetrical faults by refining power quality parameters, LVRT problem. The fault ride capability with FOSMC is good compared to FOPI and SMC controllers.

Keywords: Doubly Fed Induction Generator (DFIG), Modular Multilevel Converter (MMC), Wind Energy Conversion Systems (WECS), Machine Side Converter (MSC), Grid Side Converter (GSC), Fractional Order Super Twisting Algorithm (FOSTA), FOSTA based Sliding Mode Controller (FOSMC).

INTRODUCTION

A nonconventional power source with a lower environmental impact than fossil fuels is wind energy. It reduces the need for conventional resources like coal, oil, and natural gas, helping to mitigate the environmental damage from traditional energy production. This shift also enhances energy security by reducing dependence on imported fuels. Wind power can be applied in both small-scale settings, such as homes and farms, and large-scale wind farms. When combined with other renewables like solar, it improves the reliability of the electricity grid.

At the point of common coupling, drop in voltage reflects at stator terminals of DFIG, but the flux in stator doesn't lessen instantly. Now, the difference in speed of stator and rotor fluxes induces more voltage in rotor [1]. To direct this voltage dip, wind energy conversion system utilizes gate-controlled series capacitor (FACTS) devices [2] but they increase complexity, cost of the system. In [3], a fault current limiter along stator, series dynamic resistor in two steps at rotor side. A fault current restricter is used in [4], Resistive SFCL for Symmetrical, Asymmetrical Faults is given in [5] and modified bridge resistive type SFCL in [6]. An LVRT scheme with SFCL and RSC control [7]. Superconducting Fault Current Limiter, Dynamic Voltage Restorer have been compared for LVRT Improvement has been done in [8].

The current limiting device's ability to restrict fault current is limited by the quick response time of the DFIG, and requires an additional cooling system to manage the superconducting element. A magnetic energy storage unit and its controller has been specified in [9], SMES based Dynamic current limiter [10], a parallel connection of SMES with rotor side DFIG has been done for upgrading the LVRT Capability in [11]. A blend in which, power system stabilizer, resistive superconductor fault current limiter and static synchronous compensator for enhancing stability of a wind power generation system are studied in [12]. The effectiveness of the Modified Type Fault Current Limiter based on Nonlinear control (MBFCL) is being compared with a normally controlled fault current limiter of bridge type (BFCL) being employed to LVRT advancement in a DFIG-Based Wind Farm [13], [14] as BFCL constitutes increased power losses while operating normally due to the inherent resistance within the limiting reactor. In order to reduce dissipated heat across braking resistors, it has been sectioned in submodules at receiving end converter as in [15]. Optimised series dynamic braking resistor for uncertain faults is shown in [16]. Crowbar technology at rotor has been used in [17]. Two crowbar circuits will revamp fault ride through of DFIG [18]. Braking resistor adds power loss due to the energy dissipated as heat within the resistor during braking. Here, a Parallel/Series DC-Link Based on TAB is administered in [19]. [20] details DC link voltage regulation by an Energy Storage Device for fault ride and [21] features evolved transient stability using S Magnetic Energy Storage Unit. Energy storage device makes the system complex. Injecting voltage at common coupling point by Dynamic Voltage

Journal of Information Systems Engineering and Management
2025, 10(37s)
e-ISSN: 2468-4376
https://www.jisem-journal.com/

Research Article

Restorer (DVR) is analysed in [22]. An Unified Power Quality Conditioner with an energy storage device is bestowed in [23]. However, there is an obligation for modern control strategies to manage interactions between the UPQC/DVR and the DFIG. Modular Multilevel Converters (MMCs) offer a highly efficient and reliable solution by improving system flexibility, fault tolerance, power quality, and the management of electrical disturbances, making them an excellent option for modern high-voltage, power applications [24].

The half-bridge Modular Multilevel Converter (MMC) is ideal for HVDC systems, PV installations, and Wind Energy Systems (WES) as modularity, scalability, and high-power handling capability is achieved easily. It ensures reliable operation, dampens fault currents, and uses fewer modules for cost-effective scaling, supporting Low Voltage Ride Through (LVRT) capabilities. The MMC's arm impedance and ability to operate at higher levels enable precise control of DFIG currents, preventing control loss and disconnection during grid disturbances [25].

To intensify LVRT (Low Voltage Ride Through) capability, techniques like the Fractional Order PI Controller [26], Sliding Mode Controller [27], and Fractional Order Sliding Mode Controller (FOSMC) [28] can be used. The FOSMC significantly improves LVRT performance, stabilizes DC link voltage, and directs rotor speed, reactive power during balanced and unbalanced faults in wind farm based DFIG using Modular Multilevel Converters.

In this paper section –II deals with mathematical modeling of DFIG & MMC, section-III presents modelling, implementation of FOSMC controller for GSC converter control, discussion on simulation results, conclusions mentioned in section-IV & Section-V subsequently.

II. MATHAMATICAL MODELLING OF DFIG AND MMC.

2.1. Modelling of Doubly Fed Induction Generator (DFIG)

A space vector model of DFIM is defined in synchronous rotating frame. For this, by multiplying the voltage expression in [1], by $e^{-j\theta s}$and $e^{-j\theta r}$, respectively, we obtain the dq voltage equations:

$$\vec{v}_s^a = R_s \vec{i}_s^a + \frac{d\vec{\psi}s^a}{dt} + j\omega_s\vec{\psi}_s^a \quad (1)$$

$$\vec{v}_r^a = R_r \vec{i}_r^a + \frac{d\vec{\psi}r^a}{dt} + j\omega_r\vec{\psi}_r^a \quad (2)$$

$$\vec{\psi}_s^a = L_S i_S^a + L_m i_r^a \quad (3)$$

$$\vec{\psi}_r^a = L_r i_r^a + L_m i_s^a \quad (4)$$

The superscript "a" signifies a reference frame rotating synchronously at ω_s (synchronous speed), subscript "s", "r" indicate stator and rotor variables. Voltages, currents, fluxes are denoted as "v,", "i,","ψ." R_s R_r indicate stator and rotor resistances, respectively, while L_m,L_s and $L_r$are magnetizing, stator and rotor inductances. ω_r is rotor speed.

The equivalent electric circuit is shown in Fig-1.

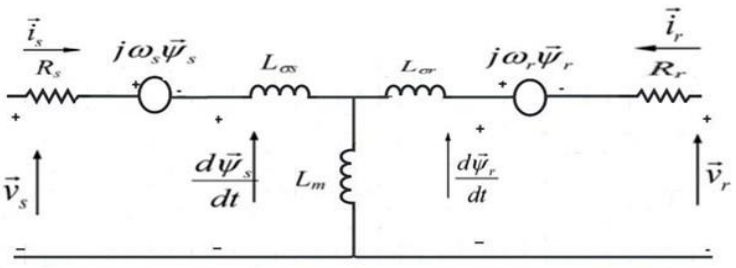

Fig-1. Equivalent Circuit of DFIG in dq reference frame

This paper employs vector control to separately regulate the components d, q of grid and rotor currents, creating dq voltage references which are subsequently transformed into abc

2.2 Modelling of Modular Multilevel Converter (MMC)

To augment the DFIG's fault tolerance during grid disturbances, traditional back-to-back six-switch Voltage Source Converters (VSCs) are being replaced by Modular Multilevel Converters (MMCs) [24]. Each MMC module consists of half-bridges and series-connected DC capacitors, operating at distinct phase angles. These modules are connected in a successive manner to rectify and invert for generating rotor currents, as shown in Fig-2.

Journal of Information Systems Engineering and Management
2025, 10(37s)
e-ISSN: 2468-4376
https://www.jisem-journal.com/

Research Article

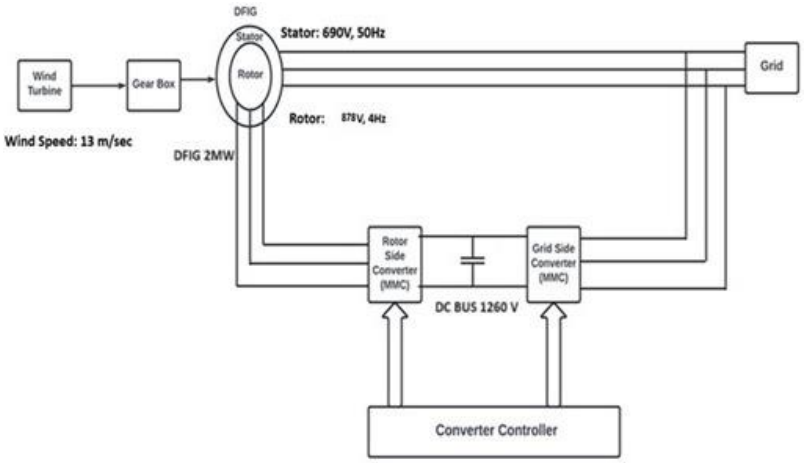

Fig-2. DFIG MMC Structure

The MMC module leg (RSC or GSC of Fig-2) includes inductors (Larm) and resistors (Rarm) to reduce current ripple from IGBT switching. Each submodule features two series-connected IGBTs and a parallel capacitor, enabling it to handle high voltages and currents [25]. The structure of an MMC submodule (SM) is shown in Fig-3.

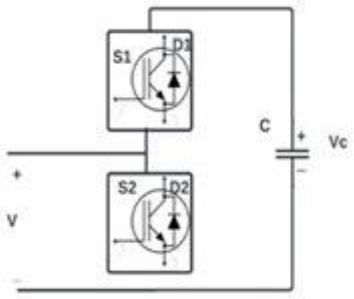

Fig-3. MMC sub module

The two MMC modules (RSC and GSC) are linked by DC capacitors (Vbus) on their DC sides. Each MMC leg contains eight submodules, providing five voltage levels, with four submodules on each side, driven independently. In a 3-phase MMC using half-bridge submodules, total number of submodules is given 2*(N–1), here N denotes the number of levels. Every submodule comprises a capacitor and two switches, and the MMC arm incorporates a series R-L impedance (Rarm and Larm), with the submodule voltage Vs synthesizing the output voltage levels.

The voltage Vsm for each submodule depends on the states of the switches S1and S2:

If switch S1=1 and S2=0, then Vsm= Vcap;

If switch S1=0 and S2=1, then Vsm= 0;

Otherwise, Vsm= 0.

In a 5-level MMC, 8 submodules, 8 capacitors, and 16 switches are required per phase. The voltage across each submodule capacitor is Vcap= Vbus/Nsm , where Nsm implies submodules present in an arm. The number of output voltage levels is Nsm+1.

Each MMC arm behaves like controlled voltage source, Varm, with its voltage amplitude (instantaneous) given by:

$$V_{arm} = \frac{SM_{active} V_{bus}}{N} \quad (5)$$

The MMC (Modular Multilevel Converter) voltage level is determined by sum of the submodule voltages Vsm, the active submodules number SMactive , and voltage sag across Rarm and Larm:

$$V_{arm} = \sum_{n=0}^{SMactive} (v_{sm}[n]) + L_{arm} \frac{diarm}{dt} + R_{arm} i_{arm} \quad (6)$$

Journal of Information Systems Engineering and Management
2025, 10(37s)
e-ISSN: 2468-4376
https://www.jisem-journal.com/

Research Article

By applying the fundamental L-C voltage-current relations v[t] = L $\frac{di[t]}{dt}$, i[t] = C$\frac{dv[t]}{dt}$, and letting C_{sminst} be the total instantaneous capacitance of the active submodules, equation (6) can be rewritten as:

V_{arm}= 1/Csminst $\int_t^0 i_{arm}\, dt + \frac{Larmdiarm}{dt} + R_{arm} i_{arm}$ (7)

Here, v[t] = L $\frac{di[t]}{dt}$, and i[t] = C $\frac{dv[t]}{dt}$ are state variables [25].

CONTROLLER DESIGN (FOSMC)

3.1 Fractional Order Sliding Mode Controller regulator design

A sliding mode control method of higher order is being adopted to alleviate the chattering problem without compromising with robustness and disturbances caused by traditional controller. Sliding mode Controller is known for its simplicity and toughness, sliding mode controller of second order with a super twisting algorithm (STA) is one of the most nonlinear strategies used in control area [28]. In juxtaposition with conventional SMC, the super twisting algorithm slashes chattering, conserves robustness of SMC. It is used in innumerable fields namely renewable energies, control and electronics because of resilience, simplicity, easy implementation and adjustment of response [29]. The equations of super twisting algorithm are written as:

$$U = \zeta e^{\gamma} \text{sign (e)} + U_1 \quad (8)$$

$$U_1 = \int \eta . \text{ sign (e)} \quad (9)$$

Where error is denoted with e, ζ and η are positive coefficients, γ = 0.5.

Equations (8), (9) streamline the working principle, understanding of STA controller. Fig.4 indicates the working principle of the controller.

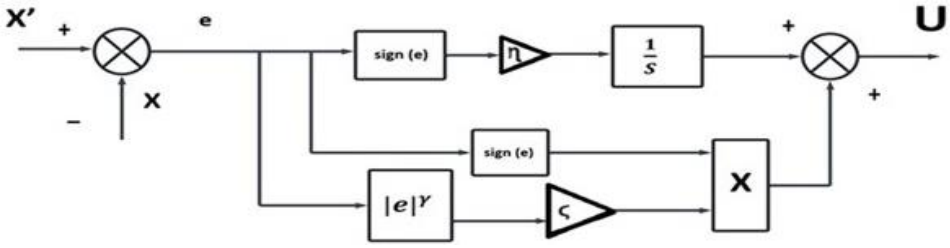

Fig-4. Conventional Super Twisting Algorithm controller.

The STA controller's use in self-operating systems like wind energy conversion systems eliminate ripples from active, reactive power and current but the standard of current is low in the network. A modification to the present method, fractional order technique is introduced to STA resulting in a new and sturdy nonlinear method, keeping STA simple and easy.

A controller that is new with STA based on fractional-order technique is used to improve the performance, efficiency of vector control strategy. As known, fractional calculus is a mathematical branch that deals with integrals and derivatives of functions with non-integer orders. This is helpful in various areas like renewable energies, based on merits compared to available methods, where flexibility of adjustment, strength are biggest advantages [30].

The proposed controller is a blend of fractional calculus and STA controller, because of easiness and simplicity of STA controller. From the suggested STA controller FOSTA controller is different [31]. Besides this, a modification of STA controller is FOSTA controller in order to attain more durability. The designed FOSTA controller's mathematical equations are written as:

$$U = [\zeta e^{\gamma} \text{sign (e)} + U_1]^{\varsigma} \quad (10)$$

$$U_1 = \int \eta . \text{sign (e)} \quad (11)$$

Where $\varsigma \neq 1$.

The fig 5 shows proposed FOSTA controller that is simple, clear, and flexible, can be implemented easily. Furthermore, this suggested method can be extended to complex systems.

Journal of Information Systems Engineering and Management
2025, 10(37s)
e-ISSN: 2468-4376
https://www.jisem-journal.com/

Research Article

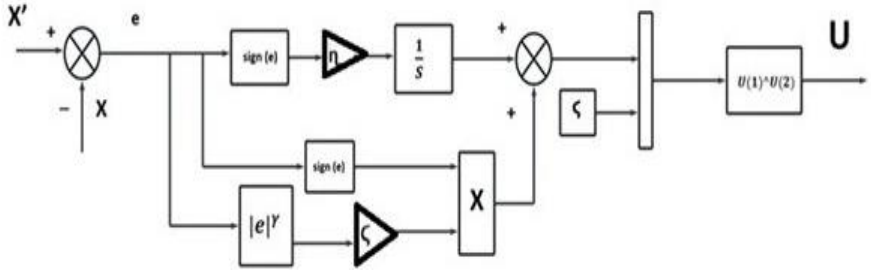

Fig-5. Proposed Fractional Order Super Twisting Algorithm based SMC (FOSMC) controller.

The later section discusses the designed controller's application at the Grid Side Converter (GSC) in order to control Low Voltage Ride through (LVRT) in a field-oriented control of DFIG-based wind energy system.

3.2. Implementation of GSC Controller for Fault Current Suppression

The controller of Grid Side Converter (GSC) handles by modulating IGBT switches to regulate the DC link voltage V_{dc}, minimizing ripple, and working in rectifier mode to charge the V_{dc} capacitor. The control structure is shown in Fig-5, which incorporates both the measured and reference signals for the system.

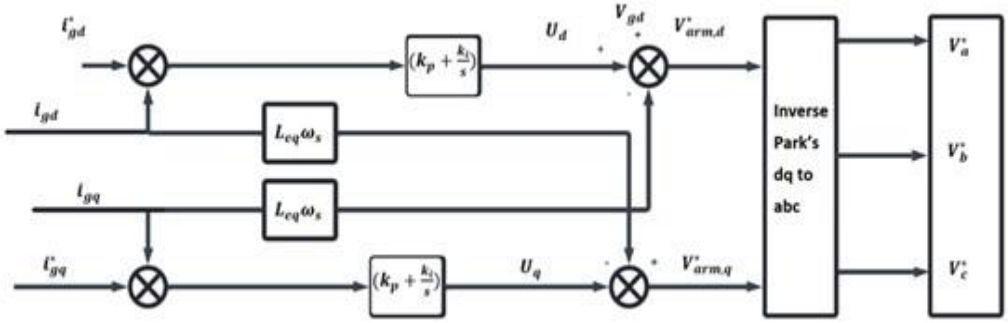

Fig-6. GSC control structure

For GSC (Grid-Side Converter) control structure, the d, q constituents of grid voltage and GSC input current are derived using Park's transformation and phase angle θ from Phase-Locked Loop (PLL). The transformation to reference frame d-q is written:

$$\begin{bmatrix} X_d \\ X_q \end{bmatrix} = \begin{bmatrix} Sin\,\theta & -Cos\,\theta & 0 \\ Cos\,\theta & Sin\,\theta & 0 \end{bmatrix} \begin{bmatrix} X_a \\ X_b \\ X_c \end{bmatrix} \quad (12)$$

Where X represents parameters like grid voltage or GSC input current. The reference dq signals for controlling the GSC IGBTs are:

$$V^*_{arm,d} = V_{gd} + U_d - I_{gq} L_{eq} \omega_s \quad (13)$$

$$V^*_{arm,q} = I_{gd} L_{eq} \omega_s - U_q \quad (14)$$

Here, Leq is the input filter inductance, ω_S is the grid angular frequency, and U_d and U_q are the current regulator components

$$U_d = (i^*_{gd} - i_{gd})(k_p + \frac{k_i}{s}) \quad (15)$$

$$U_q = (i^*_{gq} - i_{gq})(k_p + \frac{k_i}{s}) \quad (16)$$

DC voltage regulation is essential to maintain desired DC link voltage in a GSC control structure. The reference d-q current components are adjusted based on DC link voltage V_{dc} and reference voltage V^*_{dc}. A FOSTA based SMC (FOSMC) controller is used in the DC voltage control loop to obtain i^*_{gd} . The control equation is expressed as

Journal of Information Systems Engineering and Management
2025, 10(37s)
e-ISSN: 2468-4376
https://www.jisem-journal.com/

Research Article

$$\begin{bmatrix} V_a^* \\ V_b^* \\ V_c^* \end{bmatrix} = \begin{bmatrix} Sin\ \theta & Cos\ \theta \\ Sin\left(\theta - \frac{2\pi}{3}\right) & Cos\left(\theta - \frac{2\pi}{3}\right) \\ Sin\left(\theta + \frac{2\pi}{3}\right) & Cos\left(\theta + \frac{2\pi}{3}\right) \end{bmatrix} \cdot \begin{bmatrix} V_{arm,d}^* \\ V_{arm,q}^* \end{bmatrix} \quad (17)$$

The reference sinusoidal signals (V_a^*, V_b^*, V_c^*) are fed into the Phase Shift PWM (PS-PWM) technique to prompt control pulses for the GSC IGBT switches. This ensures that DC link voltage sustains at desired value,V_{dc}^*, by regulating the operation of the switches accordingly.

RESULTS AND DISCUSSION

The DFIG wind farm, based on MMC technology, is modelled in Simulink and controlled using blocks from the 'Continuous' and 'Commonly Used' libraries. The FO-PI controller is integrated via the 'FOMCON' toolbox, with simulations running on the 'Tustin' solver.

4.1 Symmetrical Fault (LLL):

In these faults, all three phases are interconnected and often grounded. The fault is balanced, with the system remaining symmetrical, meaning the phases are displaced by 120° in a three-phase system. This is the extreme fault, leading to highest current, though it happens rarely. Due to its infrequency, balanced short-circuit calculations are used to estimate these large fault currents.

For LVRT capability, a balanced fault (Voltage Sag of 90%) is introduced between the grid and DFIG wind farm. The fault resistance of R_{on} = 1 mΩ and ground resistanceR_g=10 mΩ, occurs between 3 and 3.1 seconds in a 5-second simulation. The fault scenario is controlled with an FOSMC-based GSC controller.

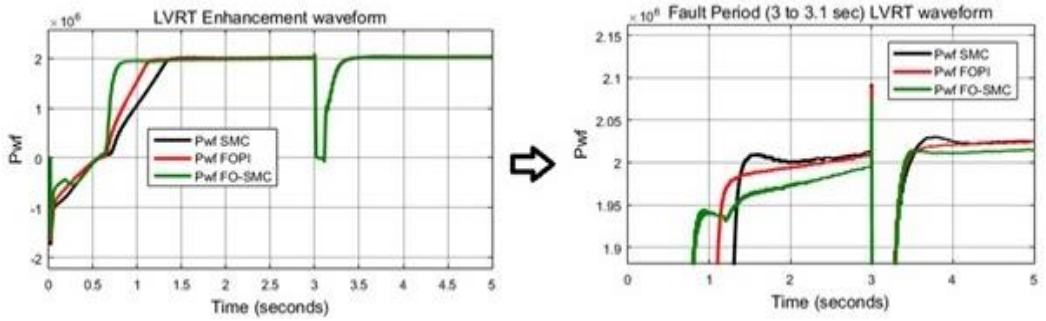

Fig-7. LVRT enhancement waveform (comparison) during symmetric fault conditions

Fig. 7 reveals that the settling time for the FOSTA based SMC (FOSMC) is 0.8 seconds, while for the Fractional Order PI (FOPI) and Sliding Mode Controller (SMC), it is 1.12 and 1.33 seconds, respectively (see Table 4). During a symmetric fault, active power (P_{wf}) drops to zero at 3 seconds and stabilizes at 2 MW by 3.5 seconds for FOSMC, compared to 3.7 and 4 seconds for FOPI and SMC

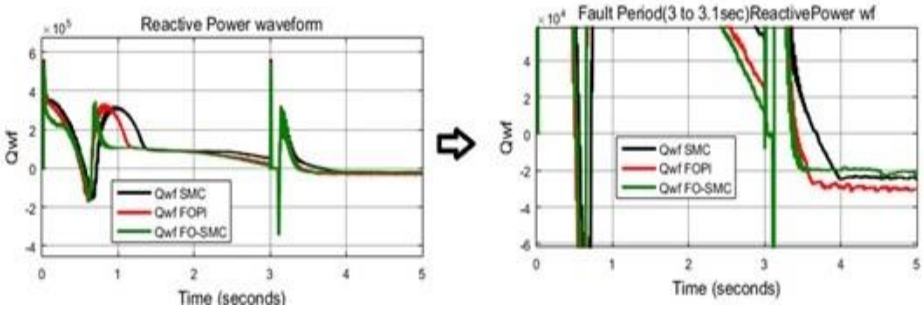

Fig-8. Comparison of Reactive Power during symmetric fault conditions

Fig. 8 and Table 4 show that the capacitor bank supplies reactive power (Q_{wf}) using the FOSTA based SMC (FOSMC) at the Grid Side Converter, which stabilizes in 0.8 seconds. In contrast, the Fractional Order Proportional Integral (FOPI) and Sliding Mode Controller (SMC) stabilize to zero in 1.15 and 1.35 seconds, respectively, before fault conditions. During a symmetric fault, FOSMC, SMC, and FOPI inject the same reactive power (Q_{wf}), but FOSMC does so in the shortest time (3.3 seconds), compared to SMC (3.4 seconds) and FOPI (3.5 seconds).

Journal of Information Systems Engineering and Management
2025, 10(37s)
e-ISSN: 2468-4376
https://www.jisem-journal.com/

Research Article

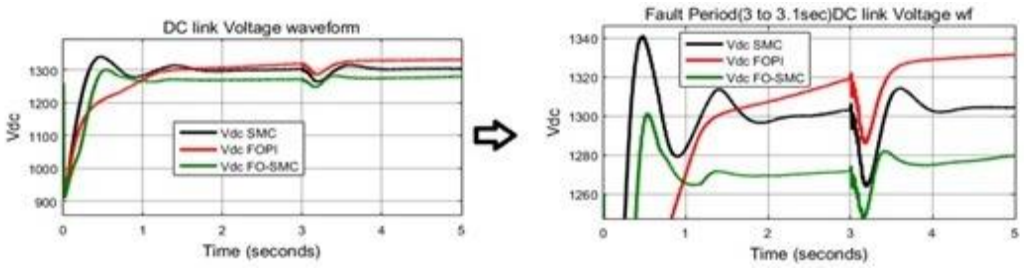

Fig-9. DC link voltage comparison during symmetric fault

Peak value of DC link voltage is1340 V for Sliding Mode Controller, 1301V for FOSTA based SMC (FOSMC) and no peak for Fractional Order PI Controller as illustrated in Fig. 9 (Table 4). At 3 seconds, a fault causes a voltage drop, and recovery is observed. After the fault, the peak voltages are 1281 V for FOSMC, 1315 V for SMC, and 1322 V for FOPI.

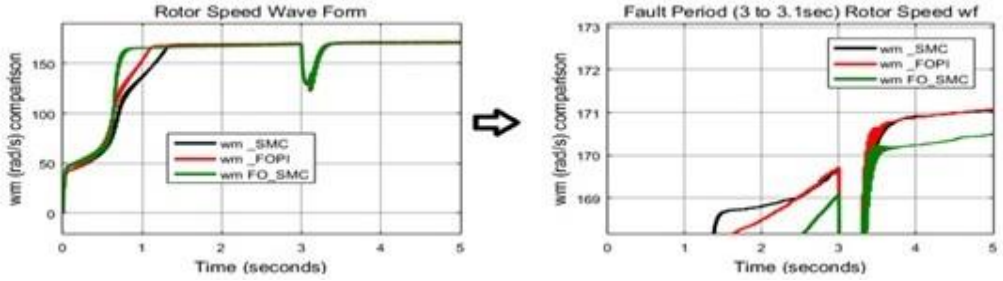

Fig-10. Rotor speed ω_m waveform during symmetric fault (comparison)

Rotor speed ω_m reaches 170.5 rad/sec at 0.8 seconds for the FOSTA based SMC (FOSMC), 171.1 rad/sec for the Fractional Order Proportional Integral (FOPI) and Sliding Mode Controllers (SMC) at 1.1 and 1.3 seconds, respectively (Table 4, Fig. 10). After the fault, FOSMC reaches 170.5 rad/sec at 3.5 seconds, compared to 171.1 rad/sec at 3.65 seconds for FOPI and SMC.

4.2 Asymmetrical Fault:

4.2.1 Line to Ground Fault (LG):

A fault (Line to Ground) with a voltage sag of 25 % occurs when phase 'A' conductor contacts the ground or neutral, often due to insulation failure. This short circuit causes current to flow to the ground, creating system imbalance, voltage fluctuations, and potential equipment damage.

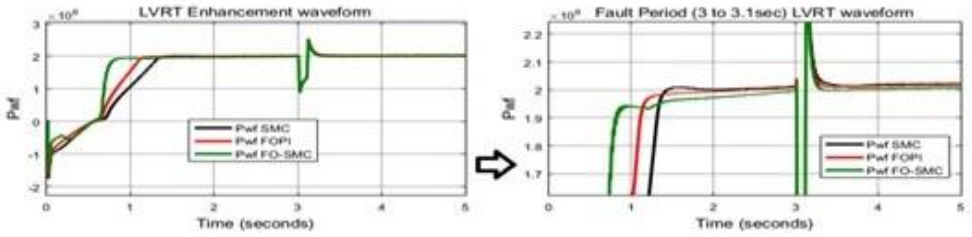

Fig-11. LVRT enhancement waveform (comparison) during fault LG condition

Fig. 11 and Table 4 show that the FOSTA based SMC (FOSMC) has a settling time of 0.8 seconds, while the Fractional Order PI (FOPI) and Sliding Mode Controllers (SMC) have settling times of 1.1 and 1.3 seconds, respectively. Due to the LG fault, active power (P_{wf}) drops to zero at 3 seconds and stabilizes at 2 MW by 3.3 seconds for FOSMC, and 2.01 MW for FOPI and SMC by 3.4 seconds.

Journal of Information Systems Engineering and Management
2025, 10(37s)
e-ISSN: 2468-4376
https://www.jisem-journal.com/

Research Article

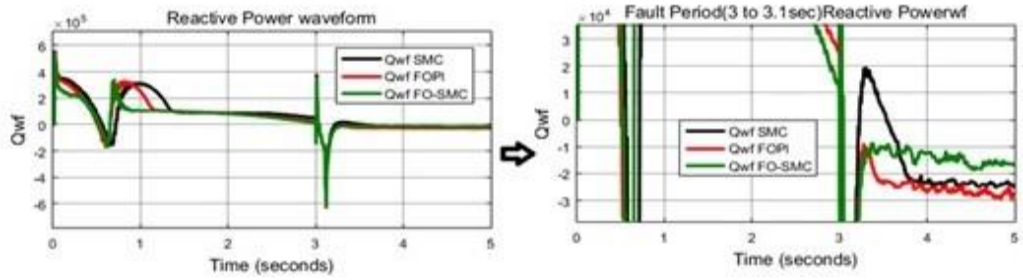

Fig-12. Comparison of Reactive Power during LG fault condition

Fig. 12 shows that the capacitor bank supplies reactive power Q_{wf}, with the Grid Side Converter controller stabilizing it to zero under normal conditions. During an LG fault, FOSMC draws the same reactive power as SMC, FOPI but in the shortest time of 0.8 sec, compared to 1.15 sec for FOPI and SMC 1.35 sec (Table 4). After the fault, Q_{wf} reaches zero at 3.3 seconds for FOSMC, at 3.5, 3.7 seconds for FOPI and SMC, respectively.

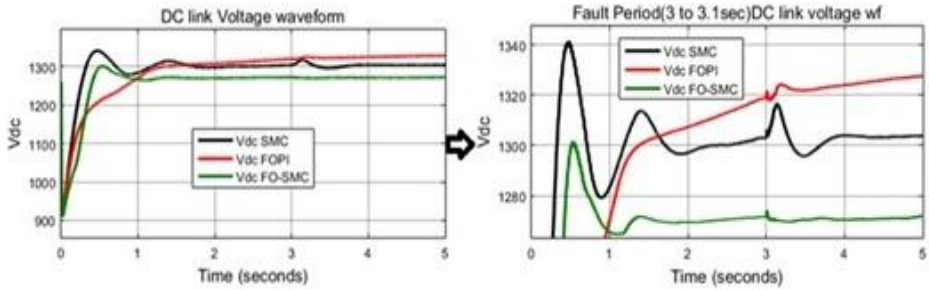

Fig-13. Comparison of DC link voltage during LG fault

Fig. 13 shows that the DC link voltage peaks at 1340V for Sliding Mode Controller (SMC), 1300V for the FOSTA based SMC (FOSMC), and no peak for the Fractional Order PI Controller (FOPI) before the fault (Table 4). During the LG fault at 3 seconds, FOSMC does not cause a voltage peak, while SMC reaches 1318V and FOPI 1322V. After the fault, SMC settles at 1304V by 3.8 seconds, and FOPI settles at 1322V by 3.5 seconds.

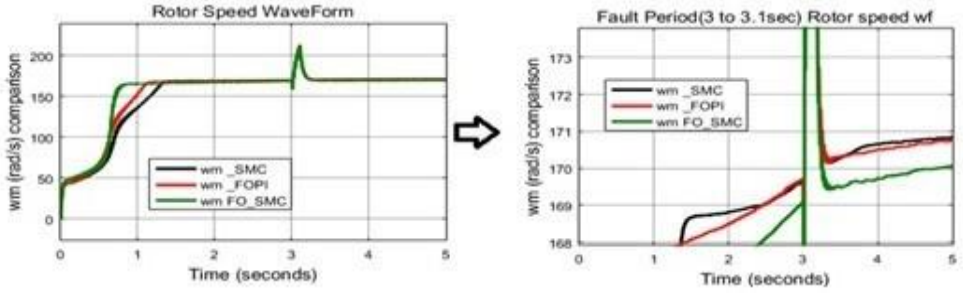

Fig-14. Rotor speed $\boldsymbol{\omega_m}$waveform (comparison) during LG fault

Rotor speed ω_m reaches 170.1 rad/sec at 0.8 seconds for FOSMC, and 170.8 rad/sec for FOPI and SMC at 1.1 and 1.3 seconds, respectively (Table 4). After the LG fault at 3 seconds, speed reaches 170.1 rad/sec at 3.3 seconds for FOSMC, compared to 170.8 rad/sec at 3.6 seconds for FOPI and SMC (Fig. 14).

Table 1: DFIG, power quality parameters with FOPI controller during and after Fault (Symmetrical and Asymmetrical).

Type of Fault	Drop in ($\boldsymbol{V_{dc}}$)	Settling Time ($\boldsymbol{T_s}$)	Drop/Rise in Active Power ($\boldsymbol{P_{wf}}$)	Settling time ($\boldsymbol{T_s}$)	Drop/Rise in Rotor Speed ($\boldsymbol{\omega_m}$)	Settling Time ($\boldsymbol{T_s}$)
LLL	1286 V	3.8 sec	0	3.3 sec	258 rad/sec	3.6 sec
LG	1322 V	3.1 sec	0.9/2.51 MW	3.55 sec	425 rad/sec	3.5 sec

Journal of Information Systems Engineering and Management
2025, 10(37s)
e-ISSN: 2468-4376
https://www.jisem-journal.com/

Research Article

Table 2: DFIG, power quality parameters with SMC controller during and after Fault (Symmetrical and Asymmetrical).

Type of Fault	Drop in (V_{dc})	Settling Time (T_s)	Drop/Rise in Active Power (P_{wf})	Settling time (T_s)	Drop/Rise in Rotor Speed (ω_m)	Settling Time (T_s)
LLL	1265 V	4 sec	0	3.3 sec	257 rad/sec	3.7 sec
LG	1317 V	3.3 sec	0.9/2.53 MW	3.55 sec	426 rad/sec	3.5 sec

Table 3: DFIG, power quality parameters with FOSTA based SMC (FOSMC) controller during and after Fault (Symmetrical and Asymmetrical).

Type of Fault	Drop in (V_{dc})	Settling Time (T_s)	Drop/Rise in Active Power (P_{wf})	Settling time (T_s)	Drop/Rise in Rotor Speed (ω_m)	Settling Time (T_s)
LLL	1248 V	3.5 sec	0	3.3 sec	260 rad/sec	3.4 sec
LG	1270 V	3.03 sec	0.95/2.5MW	3.3 sec	424 rad/sec	3.4 sec

Tables 1, 2 and 3 features the performance of Sliding Mode, Fractional Order PI and FOSTA based SMC (FOSMC) during and after the fault.

Table 4: DFIG, power quality parameters comparison with SMC, FOPI and FOSMC before Symmetrical Fault (LLL), Asymmetrical Fault (LG).

Name of the Parameter	Sliding Mode Controller (SMC)		Fractional Order PI Controller (FOPI)		FOSTA based SMC (FOSMC)	
Type of fault	LLL	LG	LLL	LG	LLL	LG
V_{dc} Peak	1340 V	1340 V	No Peak	No Peak	1300 V	1300 V
V_{dc} Settling Time	2 sec	1.8 sec	2.2 sec	1.4 sec	1.2 sec	1.2 sec
V_{dc}	1305 V	1304 V	1332 V	1328 V	1280 V	1272 V
P_{wf} Peak	No peak	No peak	No peak	No Peak	No peak	No peak
P_{wf}settling time	1.33 sec	1.33 sec	1.12 sec	1.12 sec	0.8 sec	0.8 sec
P_{wf}	2.02 MW	2.02MW	2.02 MW	2.02 MW	2.01 MW	2.01 MW
ω_m Peak	No peak	No peak	No peak	No Peak	No peak	No Peak
ω_m	171.1 rad/sec	170.8 rad/sec	171.1 rad/sec	170.8 rad/sec	170.5 rad/sec	170.1 rad/sec
ω_m Settling Time	1.3 sec	1.3 sec	1.1 sec	1.1 sec	0.8 sec	0.8 sec

CONCLUSION

This paper presents a hybrid Fractional Order Sliding Mode Controller (FOSMC) for improving LVRT and power quality in a wind energy system with DFIG and MMC. The proposed GSC controller enhances stability and robustness, using a single FOSMC regulator to manage DC link voltage ripple, rotor speed, reactive power, and LVRT. FOSMC achieves the fastest settling time for DC link voltage, rotor speed, and active power, reducing DC link voltage by 72% compared to SMC. Simulations show FOSMC outperforms with lower peak values and faster settling times under both normal and fault conditions. With a single FOSMC regulator placed in Grid Side Converter Controller, the DFIG-based system operates efficiently.The expremental results reveals that the fault ride capability of FOSMC is quite good compared to FOPI and SMC controllers.

REFRENCES

[1] H. Abu-Rub, M. Malinowski, and K. Al-Haddad, Power Electronics for Renewable Energy Systems, Transportation and Industrial Applications. Hoboken, NJ, USA: Wiley, 2014.
[2] H. A. Mohammadpour and E. Santi, "Modeling and Control of Gate-Controlled Series Capacitor Interfaced With a DFIG-Based Wind Farm," in IEEE Transactions on Industrial Electronics, vol. 62, no. 2, pp. 1022-1033, Feb. 2015, doi: 10.1109/TIE.2014.2347007.
[3] Z. -C. Zou, J. -C. Liao, Y. Lei, Z. -L. Mu and X. -Y. Xiao, "Postfault LVRT Performance Enhancement of DFIG Using a Stage-Controlled SSFCL-RSDR," in IEEE Transactions on Applied Superconductivity, vol. 29, no. 2, pp. 1-6, March 2019, Art no. 5601306, doi: 10.1109/TASC.2019.2892821.

[4] W. Guo et al., "LVRT Capability Enhancement of DFIG With Switch-Type Fault Current Limiter," in IEEE Transactions on Industrial Electronics, vol. 62, no. 1, pp. 332-342, Jan. 2015, doi: 10.1109/TIE.2014.2326997.
[5] Z. -C. Zou, X. -Y. Xiao, Y. -F. Liu, Y. Zhang and Y. -H. Wang, "Integrated Protection of DFIG-Based Wind Turbine with a Resistive-Type SFCL Under Symmetrical and Asymmetrical Faults," in IEEE Transactions on Applied Superconductivity, vol. 26, no. 7, pp. 1-5, Oct. 2016, Art no. 5603005, doi: 10.1109/TASC.2016.2574352.
[6] K. -J. Du, X. -P. Ma, Z. -X. Zheng, C. -S. Li, W. -X. Hu and K. -S. Dong, "LVRT Capability Improvement of DFIG-Based Wind Turbines With a Modified Bridge-Resistive-Type SFCL," in IEEE Transactions on Applied Superconductivity, vol. 31, no. 8, pp. 1-5, Nov. 2021, Art no. 5603005, doi: 10.1109/TASC.2021.3091114.
[7] Z. -X. Zheng, C. -J. Huang, R. -H. Yang, X. -Y. Xiao and C. -S. Li, "A Low Voltage Ride Through Scheme for DFIG-Based Wind Farm With SFCL and RSC Control," in IEEE Transactions on Applied Superconductivity, vol. 29, no. 2, pp. 1-5, March 2019, Art no. 5601005, doi: 10.1109/TASC.2019.2891687.
[8] L. Chen et al., "Comparison of Superconducting Fault Current Limiter and Dynamic Voltage Restorer for LVRT Improvement of High Penetration Microgrid," in IEEE Transactions on Applied Superconductivity, vol. 27, no. 4, pp. 1-7, June 2017, Art no. 3800607, doi: 10.1109/TASC.2017.2656624.
[9] A. M. S. Yunus, A. Abu-Siada, M. A. S. Masoum, M. F. El-Naggar and J. X. Jin, "Enhancement of DFIG LVRT Capability During Extreme Short-Wind Gust Events Using SMES Technology," in IEEE Access, vol. 8, pp. 47264-47271, 2020, doi: 10.1109/ACCESS.2020.2978909.
[10] J. Ren, X. Xiao, Z. Zheng and Z. Ma, "A SMES-Based Dynamic Current Limiter to Improve the LVRT Capability of DFIG-Based WECS," in IEEE Transactions on Applied Superconductivity, vol. 31, no. 8, pp. 1-5, Nov. 2021, Art no. 5401805, doi: 10.1109/TASC.2021.3091052.
[11] X. -Y. Xiao, R. -H. Yang, Z. -X. Zheng and Y. Wang, "Cooperative Rotor-Side SMES and Transient Control for Improving the LVRT Capability of Grid-Connected DFIG-Based Wind Farm," in IEEE Transactions on Applied Superconductivity, vol. 29, no. 2, pp. 1-5, March 2019, Art no. 0600204, doi: 10.1109/TASC.2018.2881315.
[12] M. Sarwar et al., "Stability Enhancement of Grid-Connected Wind Power Generation System Using PSS, SFCL and STATCOM," in IEEE Access, vol. 11, pp. 30832-30844, 2023, doi: 10.1109/ACCESS.2023.3262172.
[13] G. Rashid and M. H. Ali, "Nonlinear Control-Based Modified BFCL for LVRT Capacity Enhancement of DFIG-Based Wind Farm," in IEEE Transactions on Energy Conversion, vol. 32, no. 1, pp. 284-295, March 2017, doi: 10.1109/TEC.2016.2603967.
[14] M. Firouzi and G. B. Gharehpetian, "LVRT Performance Enhancement of DFIG-Based Wind Farms by Capacitive Bridge-Type Fault Current Limiter," in IEEE Transactions on Sustainable Energy, vol. 9, no. 3, pp. 1118-1125, July 2018, doi: 10.1109/TSTE.2017.2771321.
[15] X. Wang, R. Yang, Z. Shi, X. Cai, X. Shi and Y. Chen, "Coordinated Low Voltage Ride-Through of MMC-HVDC Transmission System and Wind Farm With Distributed Braking Resistors," in IEEE Access, vol. 10, pp. 87860-87869, 2022, doi: 10.1109/ACCESS.2022.3200370.
[16] J. Huang et al., "Optimized Series Dynamic Braking Resistor for LVRT of Doubly-Fed Induction Generator with Uncertain Fault Scenarios," in IEEE Access, vol. 10, pp. 22533-22546, 2022, doi: 10.1109/ACCESS.2022.3154042
[17] Z. Din, J. Zhang, Y. Zhu, Z. Xu and A. El-Naggar, "Impact of Grid Impedance on LVRT Performance of DFIG System with Rotor Crowbar Technology," in IEEE Access, vol. 7, pp. 127999-128008, 2019, doi: 10.1109/ACCESS.2019.2938207.
[18] A. M. A. Haidar, K. M. Muttaqi and M. T. Hagh, "A Coordinated Control Approach for DC link and Rotor Crowbars to Improve Fault Ride-Through of DFIG-Based Wind Turbine," in IEEE Transactions on Industry Applications, vol. 53, no. 4, pp. 4073-4086, July-Aug. 2017, doi: 10.1109/TIA.2017.2686341.
[19] J. Gu et al., "Enhanced Excitation Converter with Parallel/Series DC-Link Based on TAB for DFIG to Improve the LVRT Capability Under Severe Grid Faults," in IEEE Transactions on Power Electronics, vol. 38, no. 10, pp. 12304-12308, Oct. 2023, doi: 10.1109/TPEL.2023.3285900.
[20] Y. -W. Shen, D. -P. Ke, W. Qiao, Y. -Z. Sun, D. S. Kirschen and C. Wei, "Transient Reconfiguration and Coordinated Control for Power Converters to Enhance the LVRT of a DFIG Wind Turbine with an Energy Storage Device," in IEEE Transactions on Energy Conversion, vol. 30, no. 4, pp. 1679-1690, Dec. 2015, doi: 10.1109/TEC.2015.2449900.
[21] H. Jiang and C. Zhang, "A Method of Boosting Transient Stability of Wind Farm Connected Power System Using S Magnetic Energy Storage Unit," in IEEE Transactions on Applied Superconductivity, vol. 29, no. 2, pp. 1-5, March 2019, Art no. 5700605, doi: 10.1109/TASC.2019.2892291.
[22] R. A. J. Amalorpavaraj, P. Kaliannan, S. Padmanaban, U. Subramaniam and V. K. Ramachandaramurthy, "Improved Fault Ride Through Capability in DFIG Based Wind Turbines Using Dynamic Voltage Restorer

with Combined Feed-Forward and Feed-Back Control," in IEEE Access, vol. 5, pp. 20494-20503, 2017, doi: 10.1109/ACCESS.2017.2750738.
[23] R. H. Yang and J. X. Jin, "Unified Power Quality Conditioner with Advanced Dual Control for Performance Improvement of DFIG-Based Wind Farm," in IEEE Transactions on Sustainable Energy, vol. 12, no. 1, pp. 116-126, Jan. 2021, doi: 10.1109/TSTE.2020.2985161.
[24] S. Du, A. Dekka, B. Wu, and N. Zargari, Modular Multilevel Converters: Analysis, Control, and Applications. Hoboken, NJ, USA: Wiley, 2017.
[25] Victor R. F. B. De Souza, Luciano S. Barros, Flavio B. Costa, Guilherme P. Da Silva. "Doubly Fed Induction Generator Low Voltage Ride through Improvement through Modular Multilevel Converter", IEEE Access, vol. 10, pp. 57914-57929, 2022, doi: 10.1109/ACCESS.2022.3178960.
[26] J. López, E. Gubía, P. Sanchis, X. Roboam, and L. Marroyo, “Wind turbines based on doubly fed induction generator under asymmetrical voltage dips,” IEEE Trans. Energy Convers., vol. 23, no. 1, pp. 321-330, Mar. 2008.
[27] J. Yang, J. E. Fletcher, and J. O'Reilly, ``A series-dynamic-resistor-based converter protection scheme for doubly-fed induction generator during various fault conditions," IEEE Trans. Energy Convers., vol. 25, no. 2, pp. 422_432, Jun. 2010.
[28] Chang, X., Huang, J., Lu, F., 2017. Health parameter estimation with second-order sliding mode observer for a turbofan engine. Energies 10. http://dx.doi.org/10.3390/en10071040.
[29] Muazzam, H., Ishak, M.K., Hanif, A., Uppal, A.A., Bhatti, A., Isa, N.A.M., 2022. Virtual sensor using a super twisting algorithm based uniform robust exact differentiator for electric vehicles. Energies 15. http://dx.doi.org/10.3390/en15051773.
[30] Maaruf, M., Khalid, M., 2022. Global sliding-mode control with fractional-order terms for the robust optimal operation of a hybrid renewable microgrid with battery energy storage. Electronics 11. http://dx.doi.org/10.3390/ electronics11010088.
[31] Hamza, G., Habib, B., Sofiane, M., Ilhami, C., 2023. A new scheme of the fractional-order super twisting algorithm for asynchronous generator-based wind turbine. www.elsevier.com/locate/egyr.

APPENDIX

Parameter	Value
Rated Power, Frequency, Speed, Pole Pairs, X/R ratio (Grid)	2 MW, 50 Hz, 1500 rpm, 2, 7
Stator Resistance (R_S), Inductance (L_S)	2.6 mΩ, 2.587 mH
Rotor Resistance (R_r), Inductance (L_r)	9 mΩ, 2.587 mH
Stator, Rotor Leakage Inductance ($L_{\sigma s}$)	0.087 mH
Magnetizing Inductance ($L_{\mathbf{m}}$)	2.5 mH
DC bus voltage, Capacitor, Switching Frequency	1260 V, 100 mF, 2 kHz
MMC Arm Resistance (R_{arm}), Arm Inductance (L_{arm}), Submodule Capacitance (C_{Sm}),	0.5 Ω, 15 µH, 15 mF
kp (RSC) (PI), ki (RSC) (PI), kp (GSC) (PI), ki (GSC) (PI)	575, 4.9380 x 104, 1.1502 x 103, 4.9380 x 104
η, ζ, ς, γ (FOSMC)	0.1, 100, 0.5, 0.1

The parameters considered for simulation studies using MATLAB-Simulink for GRID, DFIG, wind Turbine and MMC.